International Journal for Modern Trends in Science and Technology
Volume 12, Issue 04, pages 1309-1321
ISSN: 2455-3778 online
Available online at: http://www.ijmtst.com/vol12issue04.html
DOI: https://doi.org/10.5281/zenodo.19697328

ANFIS-Based Intelligent Control for a Solar-Battery Powered BLDC Drive Using an Ultra High-Gain Switched-Capacitor Boost Converter

Dr.J.Srinu Naick[1] | B. Naga Pusha [2]

[1]*Professor, Dept of EEE, Chadalawada Ramanamma Engineering College, Tirupati, Andhra Pradesh, India*
[2]*PG Student, Dept of EEE, Chadalawada Ramanamma Engineering College, Tirupati, Andhra Pradesh, India*

To Cite this Article
Dr.J.Srinu Naick & B. Naga Pusha (2026). ANFIS-Based Intelligent Control for a Solar-Battery Powered BLDC Drive Using an Ultra High-Gain Switched-Capacitor Boost Converter. International Journal for Modern Trends in Science and Technology, 12(04), 1309-1321. https://doi.org/10.5281/zenodo.19697328

Article Info
Received: 19 March 2026; Revised: 17 April 2026; Accepted: 20 April 2026.

KEYWORDS

BLDC motor drive, ANFIS controller, Solar photovoltaic (PV) system, Battery energy storage, Ultra high-gain switched-capacitor boost converter, Incremental Conductance (INC) MPPT, Bidirectional DC–DC converter.

ABSTRACT

This paper develops an adaptive neuro-fuzzy inference system (ANFIS)-based smart control method for a solar-battery driven brushless dc (BLDC) motor drive using a highly-gain switched capacitor boost dc-dc converter. The proposed hybridized energy system utilizes both the photovoltaic (PV) as the primary energy source and the battery as the secondary energy storage module to provide reliable and sustainable power supply at various environment conditions. An incremental conductance (INC) maximum power point tracking (mppt) technique has been used to maximize the amount of power extracted from the pv modules. By utilizing the ultra-high gain switched capacitor boost converter, this increases the ability of voltage conversion capabilities while reduces input current ripples and device stresses. Bidirectional buck-boost converters are also utilized to efficiently charge and discharge batteries; therefore, to manage all the energies seamlessly. A novel application of ANFIS controllers has been presented instead of traditional pi controllers within a double loop control structure which comprises of an inner current loop and an outer voltage loop. The developed ANFIS controller can be able to handle system nonlinearities and variations of parameters; therefore, it provides better speed tracking performances than that of conventional PI controller in terms of less overshooting, less torque ripples and best current regulation. Entire system have been modelled and simulation performed by means of matlab/simulink tool and results demonstrated the effectiveness of ANFIS controller in comparison to conventional PI controller with respect to stability, transients responses, ripples etc. Therefore, the proposed methodology is most suitable for high performance

1. INTRODUCTION

The ever-growing worldwide demand for energy, combined with increasing concern about the environment and decreasing availability of traditional fossil fuels, has greatly hastened the transition to renewable energy systems. International efforts, such as the UN's 2030 Agenda, emphasize the need for renewable energy systems that provide both reliable and cost-effective energy; consequently, there is now strong encouragement for the world-wide application of renewable technology [1], [2]. Of many types of renewable energy systems, Solar Photovoltaic (PV) Energy Systems are considered among the most attractive due to their vastness, cleanliness, and declining cost per unit of installed capacity [3], [4]. Due to the inherently intermittent and stochastic nature of solar irradiance however, providing a constant flow of electrical power to meet variable demands associated with dynamic loads, i.e., electric drives and DC microgrids, presents great difficulties [5], [6]. One way to mitigate the problems presented by the intermittent nature of solar radiation is through the use of Energy Storage Systems (ESS). Hybrid PV-Battery Systems represent a key example of ESSs used to guarantee continued and reliable power generation by offsetting the variability in solar production and by serving as a backup during periods when solar production is low. As a result of the numerous benefits provided by such hybrid configurations (including reliability, flexibility, etc.), they are becoming increasingly popular in Electric Vehicle Propulsion Systems, Standalone Power Systems, Distributed Generation Networks and other applications [9], [10]. Thus, it is important to coordinate PV Sources and Battery Storage Systems efficiently to maintain system balance and prevent interruptions in operation. BLDC Motors are gaining popularity in many applications, including Electric Vehicles, Industrial Automation, Robotics and Households Appliances. This is mainly because of their High Efficiency, Compact Design, High Torque/Weight Ratio and Reduced Maintenance Requirements compared to conventional brush DC motors [11], [12]. Nevertheless, the Performance of BLDC Motors depends heavily on the Quality and Stability of the DC Link Voltage. Fluctuations in the Supply Voltage caused by Fluctuations in Renewable Energy Sources may cause Speed Instability, Increased Torque Ripple and Decrease System Efficiency [13], [14] . For all these reasons, it is mandatory to regulate and smooth out the DC Bus Voltage in order to achieve Optimal Performance in Renewable Energy Based BLDC Motor Drive Systems. Boost Converters are generally employed to Step Up the Low Output Voltage of PV Systems to a Suitable Level for Motor Drive Applications. However, Conventional Boost Converters have Several Limitations Including Low Voltage Gain at Moderate Duty Cycles, High Switching Stress, Increase Conduction Losses and Significant Input Current Ripple [15], [16]. To Overcome These Drawbacks, Various High-Gain Converter Topologies Have Been Proposed Such as Interleaved Boost Converters, Quadratic Converters and Coupled Inductor-Based Converters [17], [18]. While These Converters Provide Improved Voltage Gains, They Introduce Additional Challenges Such as Increased Circuit Complexity, Leakage Inductances, Electromagnetic Interference (EMI), Lack of Common Grounding Which Restrict Their Practical Implementation [19], [20]. Recently Switched-Capacitor-Based DC–DC Converters Are Emerging as an Effective Solution for Achieving High Voltage Gain Without Relaying on Magnetic Coupling. These Converters Use Capacitor-Diode Voltage Lift Techniques to Boost the Output Voltage While Operating At Moderate Duty Cycles Which Reduces Switching Losses and Device Stresses [21], [22]. Moreover, Integration of Inductor Filters in These Converters Minimize Input Current Ripples And Improve Overall System Performances. Despite These Advantages Still Remain Challenges Related To Component Optimization, Current Stresses and Ripple Reduction That Require Further Investigation [23]. Besides Efficient Power Conversion Advanced Control Strategies Are Essential for Ensuring Stable Operation and Optimizing Performance of Renewable Energy-Based Systems. MPPT Techniques Are Widely Used to Extract Max Available Power From PV Arrays Under Varying Environmental Conditions. Among Those Techniques INC Method Is Preferentially Selected Due to Its Accuracy And Fast Response Time for Tracing MPP Under Rapidly Changing Irradiance Conditions [24], [25]. Conventional Control Approaches Such as PI Controllers Are Widespread Applied in Motor Drive

Systems Due to Their Simplicity and Easy Implementation. PI Controllers Were Designed On Linear System Assumptions and Generally Fail to Deliver Satisfactory Performance in Nonlinear and Time-Varying Systems Like PV-Fed BLDC Drives. PI Controllers Show Deficiencies Such as Overshoot, Longer Settling Times and Sensitivity to Parameter Changes That Degradate Total System Performance During Dynamic Operations. Intelligent Control Techniques Such as Fuzzy Logic, Artificial Neural Networks or Hybrid Control Methods Were Proposed to Overcome Those Limitations [26]. Among Them ANFIS Technique Has Gained Great Attention Because It Can Combine Learning Ability of NN With Reasoning Ability of FL Systems. ANFIS-Based Controllers Can Effectively Manage Nonlinearity Uncertainty and Parameters Variation Which Makes Them Very Suitable for Renewable Energy-Based Application. They Offer Improvements in Dynamic Response, Reduced Overshoot, Reduced Torque Ripple and Enhanced System Stability Compared to Traditional Controllers [27]. Henceforth, the Present Work Offers an Optimized Solar-Battery Powered BLDC Drive System Incorporating Ultra-High Gain Switched-Capacitor Boost Converter for Efficient Voltage Conversion and Ripple Reduction. The Proposed Converter Was Integrated with An Input Inductor Filter to Minimize Source Current Ripple and Ensure Common Ground Configuration Which Enhances System Reliability and Compatibility with Realistic Applications. Bidirectional Buck –Boost Converter Was Employed to Manage Charge Discharge Operations Between Batteries and PV Array. This Will Allow Continuous Power Production Regardless of Varied Solar Conditions. Additionally, ANFIS-Based Intelligent Control Strategy Was Implemented Within Double Loop Framework Containing Outer Voltage Loop and Inner Current Loop. The Main Objective of Using Double-Loop Control Framework was Ensuring Precise Regulation of DC Bus Voltage, Faster Dynamic Response and Better System Stability. The Performance of ANFIS Controller Was Compared with Conventional PI Controller in Order to Highlight Superiority of ANFIS in Terms of Speed Tracking Capability of BLDC Motor, Torque Ripple Reduction and Current Regulation. Entire System was Modeled and Validated Using Matlab /Simulink. Results Demonstrated Great Improvements in Regulating Voltage Levels and Ripple Reduction as well as Global System Performance. The Proposed Architecture Provides Reliable and Efficient Solution for Renewable Energy Based Motor Drive Applications and DC Micro Grid Systems

II. SYSTEM CONFIGURATION

The proposed system will incorporate a solar photovoltaic (PV) array and battery energy storage system (bess) to supply power to both a brushless dc (BLDC) motor drive and dc load. The PV array will be the main source of electrical energy, producing a variable dc voltage depending upon ambient conditions. The PV dc voltage will then be applied to an ultra high-gain switched-capacitor boost converter. The output of this converter is a dc bus voltage that can support a variety of loads. This converter will utilize switched-capacitor and diode networks along with an input inductor to provide high voltage gain, reduce switching stresses, and minimize the input current ripple. A dc link capacitor will be placed across the output of the boost converter to help regulate and stabilize the dc bus voltage and filter out any transient or fluctuating voltages present. Once stabilized by the capacitor, the regulated dc voltage will then be provided to a voltage source inverter (vsi). The vsi will convert the regulated dc voltage into the three phase AC voltage needed to operate the BLDC motor. The inverter will use electronic commutated control of the switches based upon rotor position feedback to properly switch and run smoothly. For enhanced system reliability, a battery energy storage system will be added in series with the dc bus through a bidirectional buck-boost converter. The bidirectional buck-boost converter will enable controlled charge/discharge of the battery. When there are excessive amounts of electrical energy being generated by the PV array, the excess electrical energy can be charged into the battery. Conversely, when there is insufficient electrical energy being produced by the PV array due to reduced irradiance, the battery can discharge electrical energy back onto the dc bus so that the system remains operational. An Incremental Conductance (INC) maximum power point tracking (MPPT) algorithm will be utilized to optimize the amount of electrical energy being extracted from the PV system based upon varying operating conditions. Also, a double loop controller strategy with outer voltage loop

and inner current loop will be implemented for regulating the dc bus voltage. Finally, an adaptive neuro-fuzzy inference system (ANFIS)-based controller will be implemented to dynamically adjust its parameters based upon real time data collected from sensors, thereby improving the overall dynamic response of the system, reducing overshoots, and minimizing ripples.

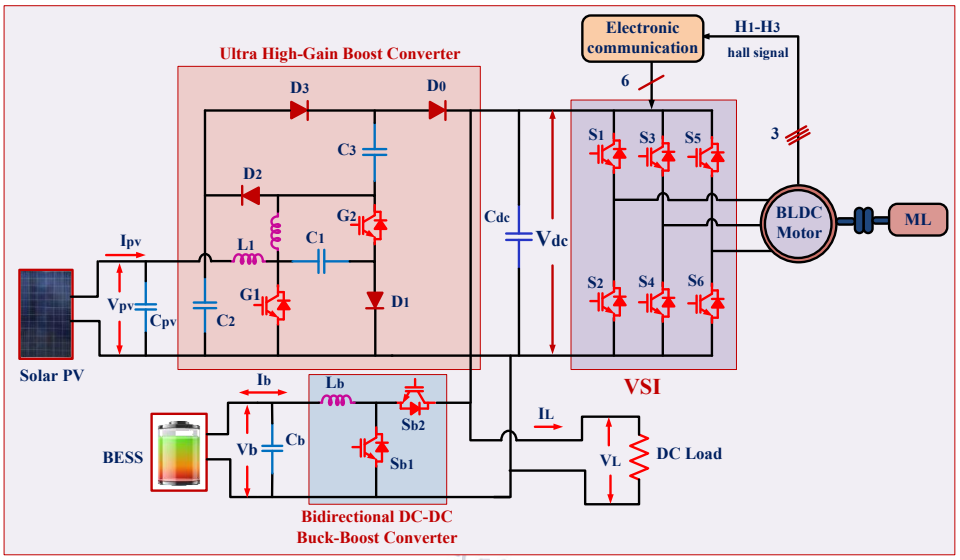

Fig. 1 Proposed system configuration solar and battery storage system for BLDC motor drive

III. Modeling and designing of solar configuration with high gain DC-DC converter

A. Solar PV Configuration

The PV panel produces very low level DC voltage, generally between 12v to 48v with varying amounts of that voltage due to many different factors. An Ultra High-Gain DC-DC Converter is therefore required to match that voltage to a high voltage load. As indicated in Fig. 3, the converter employs a multi-mode operation which includes Continous Conduction Mode (CCM) and Discontinuos Conduction Mode (DCM). The energy flow begins at the instant the switch is turned ON, where the PV panel supplies energy into the input inductor. A series of capacitors are connected via the diode-capacitor-switch configuration for additional voltage gain in stages. At the instant the switches turn OFF the inductors supply the stored energy back into the load through the diode-capacitor network. The primary mechanism for voltage boosting occurs using switched-capacitor voltage lifting. In switched-capacitor voltage lifting capacitors are placed in series to add up their individual voltages. With each successive stage the total voltage is increased by a percentage amount equal to the voltage from the previous stage. Therefore, the total voltage increases quadratically or cubically. Finally, the output is filtered with an output capacitor to produce a steady state DC high voltage across the load.

a. PV Output Current Equation:

$$I_{pv} = I_{ph} - I_0\left(e^{\frac{q(V_{pv}+I_{pv}R_S)}{nkT}} - 1\right) - \frac{V_{pv}+I_{pv}R_S}{R_{sh}} \quad (1)$$

- I_{ph}: Photogenerated current
- I_0: Reverse saturation current
- V_{pv}: PV voltage
- R_s, R_{sh}: Series and shunt resistance
- n: Ideality factor
- T: Temperature (K), q: Electron charge, k: Boltzmann constant

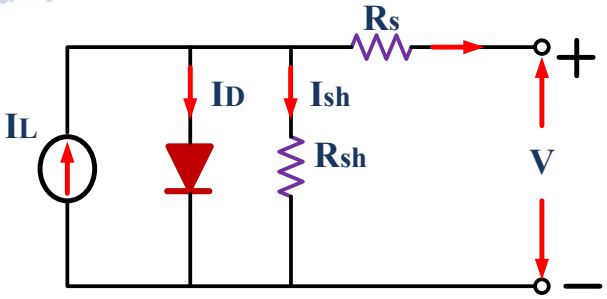

Fig. 2 equivalent model of PV solar.

B. High-Gain Switched-Capacitor Boost Converter

The Switched-Capacitor Quadratic Boost Converter (SCQBC) has been created to offer very high voltage gain. Additionally, it has low stress to its components as well as a lower level of ripple current. Therefore, it is suited to applications such as solar powered BLDC motor drives. As discussed previously, the SCQBC operates in two primary operational states: Continuous

Conduction Mode (CCM) and Discontinuous Conduction Mode (DCM), dependent upon whether or not the inductor current remains continuous throughout the switching cycle. There are two types of CCM operational states that occur within each switching cycle. They are referred to as Modes. Mode 1 is when both switches, s_1 and s_2, are ON (or active). Mode 2 occurs when both switches are OFF (or freewheeling). When operating in Mode 1, which begins at t=0, an input voltage V_i is applied directly across the inductor L_1. The inductor L_1 also receives a voltage from a charged capacitor C_1. The relationship between these voltages can be represented by:

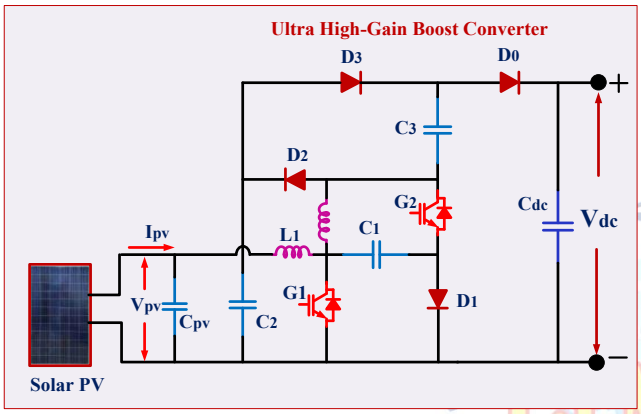

Fig.3 solar system configuration of ultra high gain switched capacitor DC-DC boost converter

$$V_{L1} = V_i \quad (2)$$

$$V_{L2} = V_{C1} \quad (3)$$

In mode two that begins at time t_1 when both the switch's are de-activated, the input source along with inductor L_1 charge capacitor C_1. and the energy from L_2 along with capacitors C_3 & C_0. supply power to the load. Inductor voltages are now:

$$V_{L1} = V_i - V_{C1} \quad (4)$$

$$V_{L2} = V_{C1} + V_{C3} - V_0 \quad (5)$$

The volt second balance method is used to evaluate the steady state behavior of inductors. This will be used to derive the expression for capacitor voltages:

$$V_{C1} = V_i(1-D) \quad (6)$$

$$V_{C2} = V_i(1-D)^2 \quad (7)$$

$$3V_{C3} = V_i(2-D)(1-D)^2 \quad (8)$$

Here, D is the duty ratio. From these capacitor voltages, the overall voltage gain of the converter in CCM can be derived as:

$$G_{CCM} = \frac{V_0}{V_i} = \frac{3-D}{(1-D)^2} \quad (9)$$

Equation shows a quadratic relationship of converter resulting in a significant increase in the voltage ratio at moderate value of duty cycle. A medium duty cycle is required to step-up a low voltage output of the photovoltaic panel (i.e. 24V), to a higher level of DC link voltage (i.e. 400 - 600 V). The current stress on all component parts of this converter can be evaluated by calculating the peak current of inductor L2 during operation in Modes 1 and 2

$$(IL_{2p})_I = \frac{V_{C1}}{L_2} DT_s \quad (10)$$

$$(IL_{2p})_{II} = \frac{V_0 - V_{C1} - V_{C3}}{L_2} D_x T_s \quad (11)$$

Equating these two peak currents at the switching boundary ensures smooth operation:

$$(IL_{2p})_I = (IL_{2p})_{II} \quad (12)$$

From this, the effective duty ratio in DCM D_x is derived:

$$D_x = \frac{D(1-D)\left(\frac{V_0}{V_i}\right)}{(1-D)^2-(3-2D)} \quad (13)$$

When the inductance current falls to zero prior to the start of the next switching cycle during DCM operations, all of the load will be supported by the output capacitor C_O. Therefore, the current through the capacitor C_O is:

$$I_{C0} = \left(\frac{1}{2} D_x IL_{2p2}\right) - I_0 \quad (14)$$

When we set the average of $I_{C0} = 0$ for a stable condition, and substitute the expression of the inductor current and duty cycle into it; we obtain an equation for calculating the DCM voltage gain.

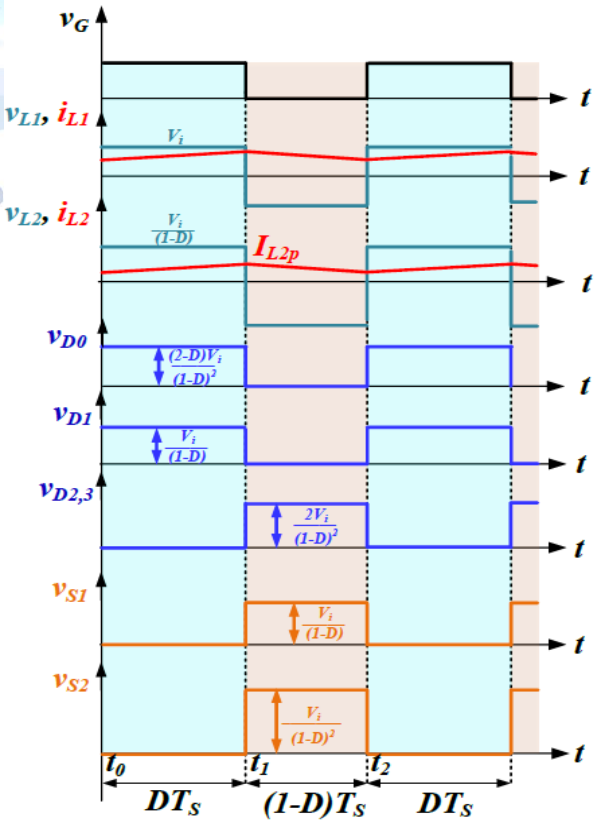

Fig. 4. Ideal operating waveforms of the SCQBC converter in one switching cycle (*t0-t2*).

C. Incremental Conductance MPPT algorithm

As illustrated in Fig.5, the incremental conductance INC method is based upon the fact that the rate of change of power with respect to voltage is zero at the max power point (MPP). Positive to the left of MPP, and negative to the right.

$$\frac{dP}{dV} = \frac{d(IV)}{dV} = I + V\frac{dI}{dV} \quad (15)$$

- At MPP: $\frac{dP}{dV} = 0 \Rightarrow \frac{dI}{dV} = -\frac{I}{V}$ (16)
- Left of MPP: $\frac{dI}{dV} > -\frac{I}{V} \Rightarrow \frac{dP}{dV} > 0$ (17)
- Right of MPP: : $\frac{dI}{dV} < -\frac{I}{V} \Rightarrow \frac{dP}{dV} < 0$ (18)

Algorithm Steps:

1. Measure $I(k)$ and $V(k)$
2. Compute $\Delta I = I(k) - I(k-1), \Delta V(k) - V(k-1)$
3. If $\Delta V = 0$
   - If $\Delta I = 0$: MPP reached → No change
   - If $\Delta I > 0$: Left of Mpp → Decrease voltage (decrease duty)
   - If $\Delta I < 0$: Right of MPP → Increase volage (increase duty)
4. $\Delta V \neq 0$
   - If $\frac{\Delta I}{\Delta V} = -\frac{I}{V}$: MPP
   - If $\frac{\Delta I}{\Delta V} > -\frac{I}{V}$: Left of Mpp → Decrease duty
   - If $\frac{\Delta I}{\Delta V} < -\frac{I}{V}$: Right of MPP → Increase duty

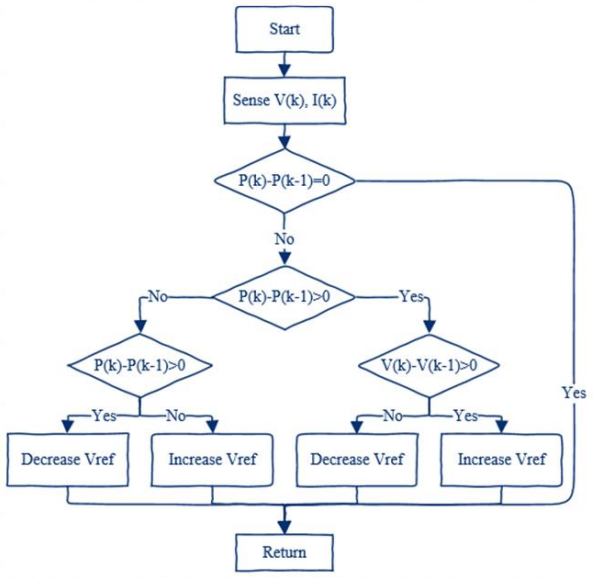

Fig. 5. Flow chart of INC algorithm of MPPT for solar conversion.

IV. Designing of Bidirectional DC-DC Buck-Boost Converter for BESS

The bidirectional DC-DC buck-boost converter (as indicated in Figure 6), will be the component responsible for determining the direction of energy flow between the solar power generator and the DC link based on the amount of solar energy available, and the needs of the motor load. The converter can operate in one of two main operating modes; boost or buck. When operating in boost mode, if the DC link voltage level is lower than the output voltage level of the PV module, then the converter will discharge the stored electrical energy of the battery into the DC link. When operating in buck mode, if the DC link voltage level is higher than the output voltage level of the PV module, then the converter will charge the battery with electrical energy that has been supplied to the DC link by the PV module. When operating in buck mode and there is an excess of electrical energy being supplied to the DC link by the PV module (i.e., $V_{PV} > V_{bat}$), the converter steps down the voltage at the DC link to match the charging profile of the battery. The main switch (S_{b1}) controls operation of this mode and is turned ON/OFF with Pulse Width Modulation (PWM) signals. While S_{b1} is ON, current flows through L_b and into C_{bat}. When S_{b1} turns OFF, D_2 allows current to flow out of C_{bat} and back onto the DC link. Thus, the charging voltage of the battery is defined by:

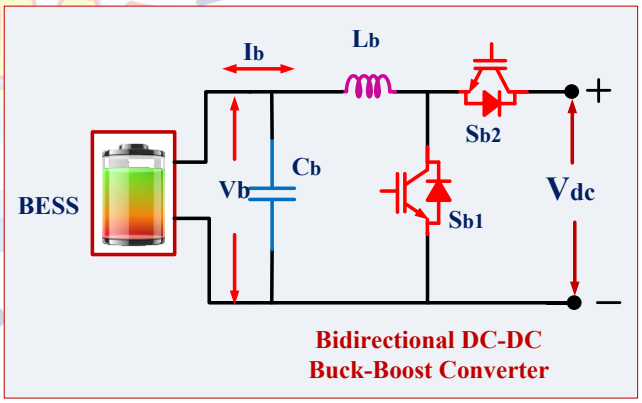

Fig.6 battery energy storage system configuration

$$V_{bat} = D \cdot V_{dc} \quad (19)$$

During discharge operation of the system when there is low PV array power production or high load demands, the dc/dc converter transitions into boost mode where the converter draws energy from the battery bank at a rate equal to that needed to maintain a constant dc link voltage V_{dc}. Since $V_{dc} > V_{bat}$, the second switch (S_{b2}) operates as an active PWM controlled device. If S_{b2} is switched on, then energy from the battery flows through L_1 to the dc link; if S_{b2} is switched off, then stored energy in L_1 is transferred to the dc link.

$$V_{dc} = \frac{V_{bat}}{1-D} \quad (20)$$

To enable smooth charge/discharge of the DC-link capacitor, to maintain stable DC-bus voltage that is

necessary for proper operation of the BLDC motor and all other DC-loads in the system; and to provide adequate margin against transients in the output due to variations in solar irradiance levels.

A. Control designing of BESS

The Double Loop PI Control Strategy, which is proposed to be used for the Solar-Battery Powered BLDC Motor Drive System provides both high accuracy and reliability when controlling the DC-bus voltage with respect to its reference value. The double loop control structure is composed of two separate cascading loops. These are referred to as the outer loop and the inner loop as shown in Fig.7. The outer loop maintains the DC-bus voltage V_{dc} at a desired reference value V_{dcref}. The outer loop accomplishes this task by sending a current reference I_{ref} signal to the inner loop. The voltage control unit determines how much error exists $e_v(t)$ in the actual measured voltage ($V_{dc}(t)$) relative to the reference voltage (V_{dcref}).

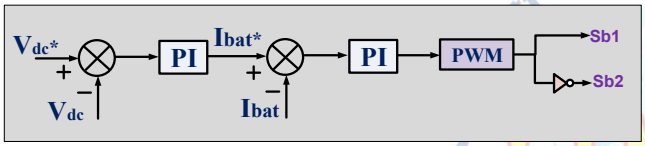

Fig. 7 Proposed energy management strategy for the BESS

$$e_v(t) = V_{dc}^{ref}(t) - V_{dc}(t) \quad (21)$$

This error is processed through a PI (Proportional-Integral) controller, whose output becomes the current reference:

$$I_{ref}(t) = K_{pv} \cdot e_v(t) + K_{iv} \cdot \int e_v(t)dt \quad (22)$$

The inner loop determines whether the reference current i_{ref} being followed closely by the actual current i_{dc} through the inductors to the load, with the resultant difference from these two currents, used by a PI (Proportional-Integral) controller for current to calculate the best possible switching sequence to follow the current reference as tightly as possible even when there are rapid changes in the load.

Current Error:

$$e_v(t) = I_{ref}(t) - I_{dc}(t) \quad (23)$$

PI Current Controller Output (duty ratio control):

$$D(t) = K_{pi} \cdot e_i(t) + K_{ii} \cdot \int e_i(t)\,dt \quad (24)$$

k_{pv} and k_{iv} represent the proportional and integral values for the voltage controllers and k_{pi} and k_{ii} are the proportional and integral gain values for the current controllers. This hierarchical control scheme provides both quick transient response (current control), and good steady-state performance (voltage regulation). As such, this type of control strategy is well-suited for use in renewable energy-based systems where you have power electronic components that will require high-quality current/voltage control such as the BLDC motor drive in your design.

V. Controller and Designing of BLDC motor drive

The BLDC motor needs the proper sequence of voltages to the stator windings based on the rotor's position detected by hall sensors for proper switching of the inverter. Proper switching allows the generated stator magnetic field to lead the rotor magnetic field creating continuous torque as depicted in Figure 8. The inverter will operate in a six step commutating mode where two phases are active at all times while one phase is always inactive. This operating mode produces a trapezoid shaped waveform of current which is synchronized to the back emf produced by the motor. The back emf varies as the rotor turns and therefore so does the applied voltage and current. The coordinated application of voltage, current, and commutated angle of the motor results in both an efficient and smooth operation of the motor regardless of load or supply condition.

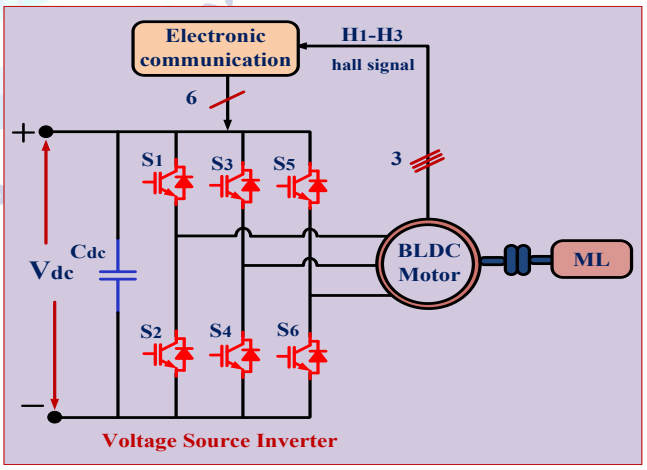

Fig.8 BLDC motor drive configuration

A. Designing of BLDC Motor

The Brushless D.C. (B.L.D.C.) Motor is an Electrically Commutated Machine where a rotating magnetic field is produced by energizing the Stator Winding in a Specific Sequence. As a result of this energization, the Rotor Follows Due To Permanent Magnets. In addition to exhibiting Trapezoidal Back E.M.F., the B.L.D.C. Motor is Often Controlled Using Feedback From Hall Effect Sensors to Determine the Position of the Rotor. The

Electrical Dynamics of the B.L.D.C. Motor are Governed By Kirchoff's Voltage Law Applied to Each Stator Winding.

$$V_a = Ri_a + L\frac{di_a}{dt} + e_a \quad (25)$$

$$V_b = Ri_b + L\frac{di_b}{dt} + e_b \quad (26)$$

$$V_c = Ri_c + L\frac{di_c}{dt} + e_c \quad (27)$$

Where:

- $V_{a,b,c}$: Terminal voltages of phases a, b, and c
- $I_{a,b,c}$: Phase currents
- R: Resistance per phase
- L: Inductance per phase
- $e_{a,b,c}$: Back EMFs of each phase

The back EMF for each phase is dependent on the rotor electrical angle θ and angular velocity ω, and for a BLDC motor, it follows a trapezoidal profile:

$$e_a = K_e \cdot f_a(\theta) \cdot \omega \quad (28)$$

$$e_b = K_e \cdot f_b(\theta) \cdot \omega \quad (29)$$

$$e_a = K_e \cdot f_c(\theta) \cdot \omega \quad (30)$$

Where K_e is the back EMF constant and $f_{a,b,c}(\theta)$ are trapezoidal functions depending on rotor position sensed using Hall sensors.

B. Mechanical Modeling of BLDC Motor

The rotor dynamics follow Newton's second law of motion, balancing the electromagnetic torque with the load and frictional torque. The mechanical equation is:

$$J \cdot \frac{d\omega}{dt} + B \cdot \omega = T_e - T_L \quad (31)$$

Where: J: Rotor moment of inertia, B: Friction coefficient, ω: Rotor angular speed (rad/s), Te: Electromagnetic torque, TL: Load torque

The electromagnetic torque generated by the BLDC motor is a function of the back EMF and the current in each phase:

$$T_e = \frac{1}{\omega}(e_a i_a + e_b i_b + e_c i_c) \quad (32)$$

This shows that torque is directly proportional to the product of back EMF and stator current.

B. ANFIS-Based Speed Controller for BLDC Motor

In a proposed solar- and battery-powered BLDC motor drive system, a fast speed regulation is required to maintain a high dynamic behavior of the BLDC motor and minimize the torque ripples and stabilize the operation during different working points. For these purposes, in addition to using an adaptive neuro-fuzzy inference system (ANFIS) based on a fuzzy logic speed controller in the outer control loop, the current controller will be located at the inside control loop as shown in Fig.9. ANFIS controller has better characteristics than the PI controllers in terms of performance when the operating point varies non-linearly or periodically over time, as it often happens in renewable-energy based drive systems. The inputs of the ANFIS speed controller are the error of speed (the difference between the desired speed $\omega^*(t)$ and the actual speed of the motor $\omega(t)$ and the change of speed error.

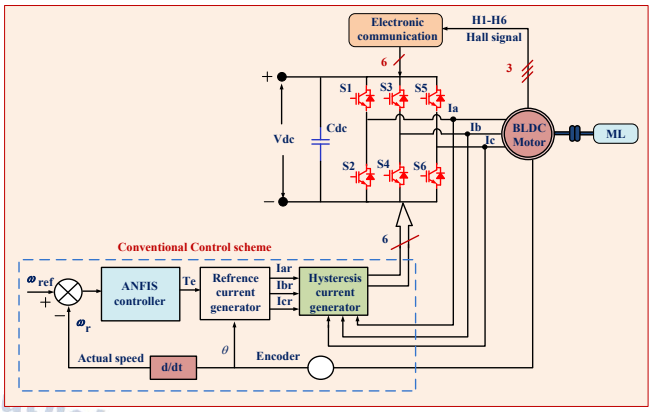

Fig.9 speed controller designing of BLDC motor drive

$$e_\omega(t) = \omega*(t) - \omega(t) \quad (33)$$

The change in speed error is expressed as

$$\Delta e_w(t) = e_\omega(t) - e_\omega(t-1)$$

These two signals are applied to the ANFIS controller, which generates the control output corresponding to the reference torque or reference current required for the motor. Thus, the ANFIS controller output can be represented as

$$i^*_{ref} = f\big(e_\omega(t), \Delta e_\omega(t)\big)$$

Where f(·) represents the non-linear mapping defined by the ANFIS structure. The generated reference current i^*_{ref} is then supplied to the reference current generator to produce the phase current references for the BLDC motor. These current references are compared with the measured phase currents and a hystersis current controller is used to provide appropriate switching pulses for the VSI.

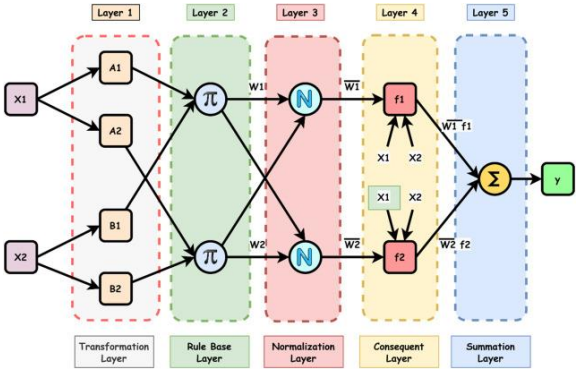

Fig.10 ANFIS-optimized control

The ANFIS controller combines the linguistic reasoning of a Fuzzy Inference System with the adaptive learning of Neural Networks. A typical controller comprises five layers. The first layer converts the input variables $e_\omega(t)$, and $\Delta e_w(t)$ into fuzzy membership degrees. The second layer forms fuzzy rules using the input combinations as demonstrated in Figure 10. The third layer normalizes the firing strength of each rule. The fourth layer computes the consequent parameter values, and the fifth layer computes an overall output value by adding up all the individual rule outputs. For a two-input ANFIS structure, the fuzzy if–then rules can be expressed as follows:

$Rule\ 1: If\ e_\omega$ is A_1 and Δe_ω is B_1, then $y_1 = p_1 e_\omega + q_1 \Delta e_\omega + r_1$

$Rule\ 2: If\ e_\omega$ is A_2 and Δe_ω is B_2, then $y_2 = p_2 e_\omega + q_2 \Delta e_\omega + r_2$

where A_i and B_i are the fuzzy sets associated with the inputs, and P_i, q_i, and r_i are the consequent parameters of the Sugeno-type fuzzy model. The firing strength of each rule is computed as

$$w_i = \mu A_i(e_\omega)\mu B_i(\Delta e_\omega)$$

where μA_i and μB_i denote the membership functions of the corresponding fuzzy sets. The normalized firing strength is given by

$$\bar{w}_i = \frac{w_i}{\Sigma_i \omega_i}$$

Accordingly, the overall output of the ANFIS controller is expressed as

$$i^*_{ref}(t) = \sum_i \bar{w}(p_i e_w + q_i \Delta e_\omega + r_i)$$

This output determines the required reference current for producing the electromagnetic torque necessary to track the desired speed. The electromagnetic torque of the BLDC motor is proportional to the phase current and is expressed as

$$T_e(t) = k_t i(t)$$

where k_t is the motor torque constant and $i(t)$ is the motor current. The mechanical dynamics of the BLDC motor are governed by

$$J\frac{d_\omega(t)}{dt} + B_\omega(t) = T_e(t) - T_L(t)$$

where J is the rotor inertia, B is the viscous damping coefficient, and $T_L(t)$ is the load torque.

The ANFIS controller is trained based on input/output data collected from the BLDC motor drive when operated at various working points. During training, the premisses (premise) and consequences (consequent) of the premises and conclusions are modified so that it can accurately model the non-linear relation between the speed error signals and required control actions. Therefore, it adapts well to changes in parameters of the solar battery powered drive system due to nonlinear characteristics or disturbances. Compared to the PI controller used conventionally, this speed controller has some benefits. It produces fast transient responses; it has less overshooting, and a shorter settling time than its PI counterpart. This is because it also demonstrates increased robustness in the presence of load and source disturbance. Additionally, the ANFIS controller reduces the torque ripples as well as the current oscillations to improve the total performance of the BLDC motor drive. For these reasons, the ANFIS based control methodology is very suitable for renewable energy powered BLDC drives with dominant nonlinear behavior and varying operation conditions.

VI. Simulation Results and Discussion

A. Dynamic Performance Analysis of Solar-Battery Powered BLDC Drive under Variable Irradiance and Speed Conditions

The proposed solar and battery powered BLDC motor drive system has been modelled and simulated in MATLAB/Simulink over a total time of 1 second to assess the systems' transient performance characteristics and ability to share power based on changing environmental and load operating conditions as shown in Fig.11. In addition to a 8 kW solar photovoltaic array and a 5 kW battery energy storage system; the system comprises of a 2 kW BLDC motor and a 3.2 kW DC load. A high gain DC-DC Boost Converter was used to extract the solar power. This converter also had an incremental conductance maximum power point tracking (MPPT) algorithm to maximise the extraction of solar power regardless of the solar irradiance level. The first stage of testing was to run the solar system at full capacity, which was achieved when the solar irradiance was set at 1000 W/m² between 0 and 0.2 seconds. As expected, during this phase, the solar system was able to provide sufficient power to meet the demand of both the BLDC motor and the DC Load. The same could be said for the battery charging. However, as the irradiance decreased from 1000 W/m² to 500 W/m² over the time interval between 0.2 and 0.3 seconds, the reduction in solar power resulted in the battery discharging to offset the shortfall. Thus providing an uninterrupted power supply to both the BLDC Motor and DC Load. With

further reductions in the irradiance, from 500 W/m² to 300 W/m² over the time interval of 0.3 and 0.4 seconds, there was a corresponding increase in the rate of battery discharge. This was necessary to maintain the required load demand and thus ensure reliability of the overall system. When the irradiance dropped to zero W/m² over the time interval of 0.4 to 0.5 seconds; i.e., it was completely dark, then the battery became solely responsible for supplying power to the complete system. Under these extreme conditions, it was possible for the battery to support both the BLDC Motor and DC Load without suffering any loss of performance. It can be seen that throughout this duration, the overall system was capable of dynamically balancing power supplied by the solar source and the battery source while maintaining a steady state DC Bus Voltage. Also, throughout this duration, the BLDC Motor underwent variable speed operation, so that the overall system's stability and controller response were tested. Over the initial time period of 0 to 0.5 seconds, the motor speed remained constant at 1000 RPM. Subsequently, from 0.5 to 0.65 seconds, the motor speed increased from 1000 to 1500 RPM, with a subsequent increase in speed from 1500 to 2000 RPM being made over the next time interval of 0.65 to 0.85 seconds. Finally, from 0.85 to 1 second, the motor speed increased once again from 2000 to 3000 RPM. It should be noted that despite the large variations in mechanical speed and load conditions experienced by the BLDC Motor during these tests, the proposed control strategy ensured that smooth operation continued to exist along with effective torque responses and low overshoots.

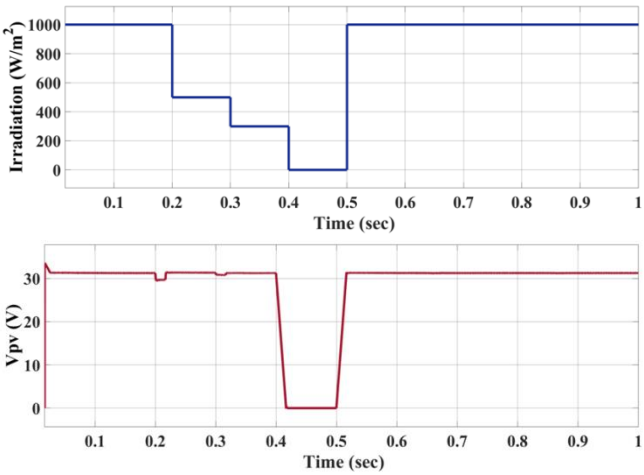

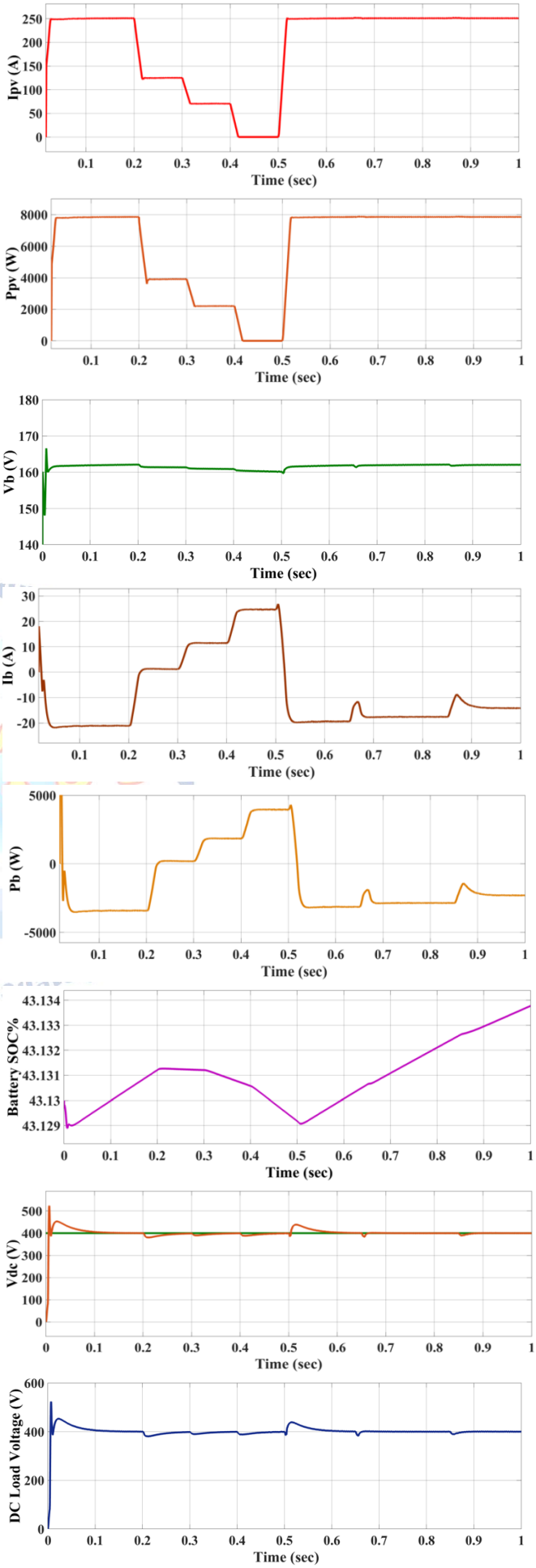

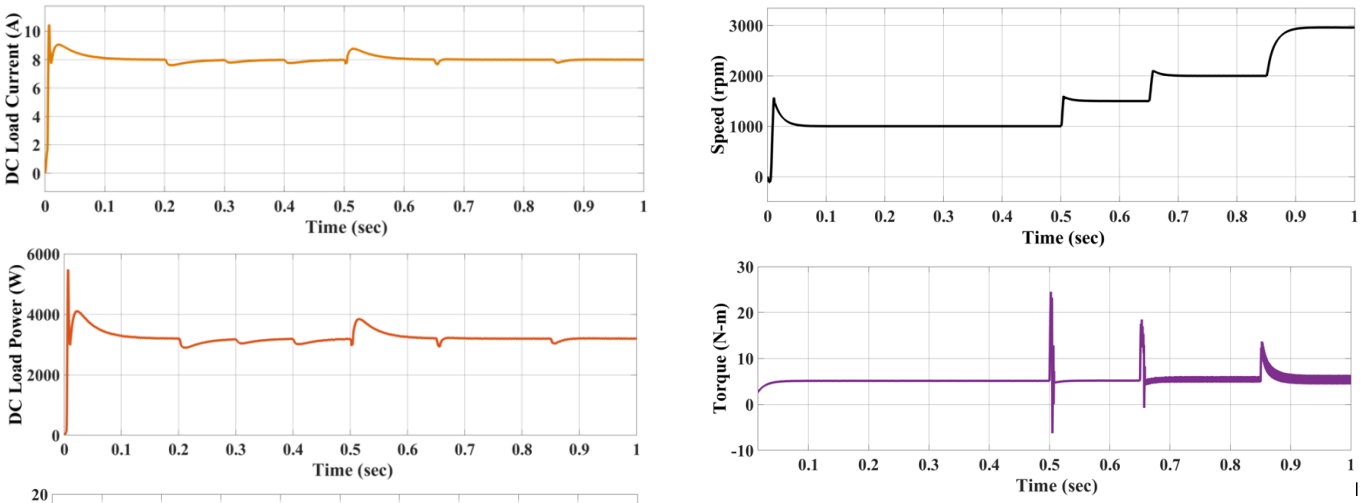

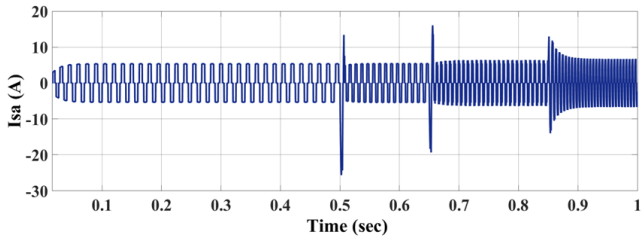

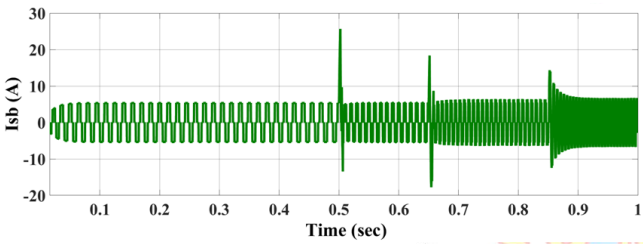

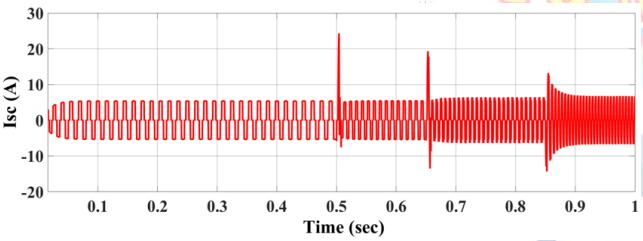

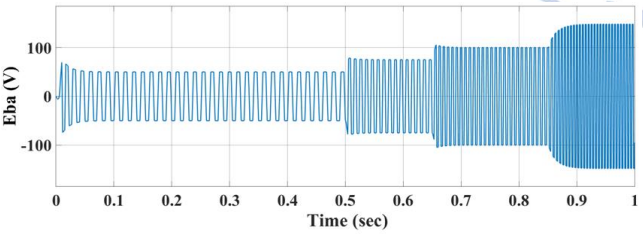

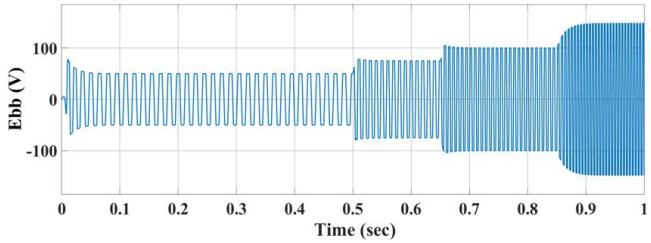

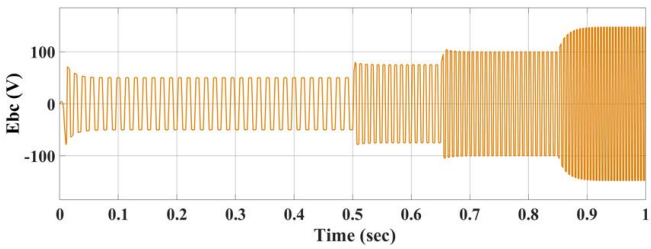

Fig.11. Simulation results of Dynamic Performance Analysis of Solar-Battery Powered BLDC Drive under Varying Irradiance and Speed Conditions

B. Comparative Performance Analysis of PI and ANFIS Controllers

The transient responses of the PI and ANFIS controllers can be easily seen from the simulation data and show how well the two control methods will track a given reference speed. At each of the three reference speed steps (500 rpm to 1500 rpm at 0.25 s, 2000 rpm at 0.5 s, and 3000 rpm at 0.75 s), the PI controller has a larger amount of overshoot than the ANFIS controller and takes longer to settle down at each transition. The reason why the PI controller shows these characteristics is because it does not have enough flexibility to quickly respond to large amounts of nonlinearity as shown in the BLDC motor. However, the ANFIS controller performs much better and has less overshoot while having a faster settling time. This is due to the ability of the ANFIS controller to learn about its operating environment over time through an adaptive process. Therefore, this helps the ANFIS controller to perform very well under conditions where there are many types of nonlinearities present in the system as shown in Fig.12. A comparison was also made using the electromagnetic torque output of the motor. As previously mentioned, when transitioning from one speed to another, the PI controller produced significantly greater torque ripples and had several oscillations before achieving a steady-state condition. However, the ANFIS controller greatly reduced the torque ripple and suppressed most of the oscillation associated with the torque output. Reducing the amplitude of torque ripples is important because excessive ripples can reduce the overall life expectancy of motors and increase the stress experienced by them.

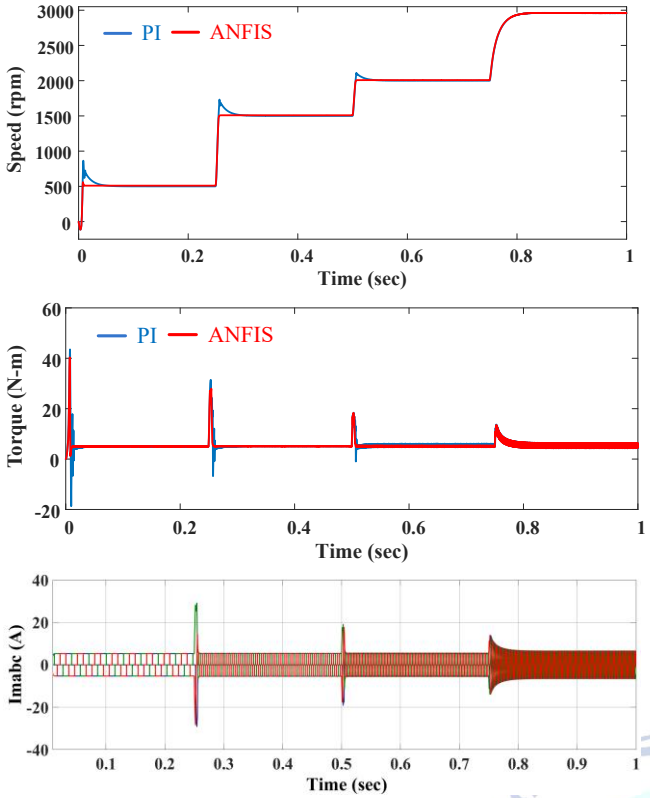

Fog.12 Simulation Results and Comparative Performance Analysis of PI and ANFIS Controllers

VII. Conclusion

A solar/battery powered BLDC motor drive system was successfully developed and evaluated as part of this research project utilizing an ultra-high gain switched capacitor boost converter capable of minimizing the ripple content on the source current. As a result of integrating the photovoltaic array with battery based energy storage, it is possible to provide a continuous and reliable supply of power to both the BLDC drive and DC loads when the source power is being provided by solar arrays under variable solar irradiance conditions. Additionally, the INC MPPT method utilized provides for extracting the maximum amount of power from the photovoltaic source while the ultra-high gain switched capacitor boost converter minimizes both source current ripple and voltage stress on all devices within the system resulting in increased efficiency and robustness of the entire system. The use of the bidirectional buck/boost converter also enables smooth charging/discharging operations of the batteries providing a means to maintain a balance of power between the two potential power sources. Finally, the double loop control strategy provides for effective regulation of the DC link voltage via coordinated voltage and current control which improves the dynamic performance and stability of the entire system. Simulations were conducted utilizing MATLAB/SIMULINK that demonstrated the capability of the system to operate at different speeds and meet various load requirements while maintaining a consistent flow of power and regulating the DC bus voltage. This study demonstrates that the proposed configuration represents a viable and cost-effective solution for electrical drives and DC loads supplied by renewable energy resources.

Conflict of interest statement

Authors declare that they do not have any conflict of interest.

References

[1] Kala Meah, Steven Fletcher and Sadrul Ula, "Solar Photovoltaic Water Pumping for Remote Locations," Renewable and Sustainable Energy Reviews, vol. 12, no. 2, pp. 472-487, February 2008.

[2] C. Gopal, M. Mohanraj, P. Chandramohan and P. Chandrasekar, "Renewable Energy Source Water Pumping Systems—A Literature Review," Renewable and Sustainable Energy Reviews, vol. 25, pp. 351-370, September 2013.

[3] J. V. Mapurunga Caracas, G. De Carvalho Farias, L. F. Moreira Teixeira and L. A. de Souza Ribeiro, "Implementation of a High-Efficiency, High-Lifetime, and Low-Cost Converter for an Autonomous Photovoltaic Water Pumping System," IEEE Transactions on Industry Applications, vol. 50, no. 1, pp. 631-641, Jan.-Feb. 2014.

[4] Mehmet Akbaba, "Matching Induction Motors to PVG for Maximum Power Transfer," Desalination, vol. 209, no. 1–3, pp. 31-38, 2007.

[5] A. Boutelhig, Y. Bakelli, I. Hadj Mahammed and A. Hadj Arab, "Performances Study of Different PV Powered DC Pump Configurations for an Optimum Energy Rating at Different Heads Under the Outdoor Conditions of a Desert Area," Energy, vol. 39, no. 1, pp. 33- 39, March 2012.

[6] N. Chandrasekaran, G. Ganeshprabu and K. Thyagarajah, "Comparative Study of Photovoltaic Pumping System Using a DC Motor and PMDC Motor," International Conference on Advances in Engineering, Science and Management (ICAESM), pp. 129-132, 30-31 March 2012.

[7] Abdelmalek Mokeddem, Abdelhamid Midoun, D. Kadri, Said Hiadsi and Iftikhar A. Raja, "Performance of a Directly-Coupled PV Water Pumping System," Energy Conversion and Management, vol. 52, no. 10, pp.3089-3095, September 2011.

[8] S. Henneberger, S. Van Haute, K. Hameyer and R. Belmans, "Submersible Installed Permanent Magnet Synchronous Motor for a Photovoltaic Pump System," IEEE International Electric Machines and Drives Conference Record, pp. WB2/10.1-WB2/10.3, 18-21 May 1997.

[9] R. Chenni, L. Zarour, A. Bouzid and T. Kerbach, "Comparative Study of Photovoltaic Pumping Systems Using a Permanent Magnet Synchronous Motor (PMSM) and an Asynchronous Motor (ASM)," Rev. Energy Ren. Vol. 9, pp. 17-28, 2006.

[10] M. Dubey, S. Sharma and R. Saxena, "Solar PV Stand-alone Water Pumping System Employing PMSM Drive," IEEE Students' Conference on Electrical, Electronics and Computer Science, pp. 1-6, 2014.
[11]S. Saravanan and N. R. Babu, "Design and Development of Single Switch High Step-Up DC–DC Converter," in *IEEE* , vol. 6, no. 2, pp. 855-863, June 2018.
[12] P. K. Maroti, S. Padmanaban, J. B. Holm-Nielsen, M. Sagar Bhaskar, M. Meraj and A. Iqbal, "A New Structure of High Voltage Gain SEPIC Converter for Renewable Energy Applications," in *IEEE Access*, vol. 7, pp. 89857-89868, 2019.
[13] Baba, MF, Giridhar, AV and Narasimharaju, BL, "Active switched-capacitor based ultra-voltage gain quadratic boost DC-DC converters" in *Int J Circ Theor Appl*, 2023, 51 (3): 1389- 1416.
[14] T. S. Ambagahawaththa, D. Nayanasiri, A. Pasqual and Y. Li, "A Design Methodology to Synthesize First Degree Single-Path Hybrid DC–DC Converters," in IEEE Transactions on Power Electronics, vol. 37, no. 10, pp. 12336-12345, Oct. 2022.
[15] T. S. Ambagahawaththa, D. Nayanasiri, A. Pasqual and Y. Li, "Nonisolated DC–DC Power Converter Synthesis Using Low- Entropy Equations," in IEEE Journal of Emerging and Selected Topics in Power Electronics, vol. 10, no. 6, pp. 6457-6469, Dec. 2022.
[16] V. Karthikeyan, S. Kumaravel and G. Gurukumar, "High Step-Up Gain DC–DC Converter With Switched Capacitor and Regenerative Boost Configuration for Solar PV Applications," in *IEEE Transactions on Circuits and Systems II: Express Briefs*, vol. 66, no. 12, pp. 2022-2026, Dec. 2019.
[17] S. A. K. H. Mozaffari Niapour, S. Danyali, M.B.B. Sharifian and M.R. Feyzi, "Brushless DC Motor Drives Supplied by PV Power System Based on Z-Source Inverter and FL-IC MPPT Controller," Energy Conversion and Management, vol. 52, no. 8–9, pp. 3043-3059, 2011.
[18] A. Terki, A. Moussi, A. Betka and N. Terki, "An Improved Efficiency of Fuzzy Logic Control of PMBLDC for PV Pumping System," Applied Mathematical Modelling, vol. 36, no. 3, pp. 934-944, March 2012.
[19] M. Ouada, M.S. Meridjet and N. Talbi, "Optimization Photovoltaic Pumping System Based BLDC Using Fuzzy Logic MPPT Control," Int. Renewable and Sustainable Energy Conf., pp. 27-31, 7-9 March 2013.
[20] Zhou Xuesong, Song Daichun, Ma Youjie and Cheng Deshu, "The Simulation and Design for MPPT of PV System Based on Incremental Conductance Method," WASE International Conference on Information Engineering (ICIE), vol. 2, pp. 314-317, 14-15 Aug. 2010.
[21] Issam Houssamo, Fabrice Locment and Manuela Sechilariu, "Experimental Analysis of Impact of MPPT Methods on Energy Efficiency for Photovoltaic Power Systems," International Journal of Electrical Power & Energy Systems, vol. 46, pp. 98-107, March 2013.
[22] B. Subudhi and R. Pradhan, "A Comparative Study on Maximum Power Point Tracking Techniques for Photovoltaic Power Systems," IEEE Transactions on Sustainable Energy, vol. 4, no. 1, pp. 89-98, Jan. 2013.
[23] T. K. Soon and S. Mekhilef, "Modified Incremental Conductance MPPT Algorithm to Mitigate Inaccurate Responses Under Fast-Changing Solar Irradiation Level," Solar Energy, vol. 101, pp. 333-342, 2014. [24] Kok Soon Tey and S. Mekhilef, "Modified Incremental Conductance Algorithm for Photovoltaic System Under Partial Shading Conditions and Load Variation," IEEE Trans. Ind. Electron., vol.61, no.10, pp.5384-5392, Oct. 2014.
[24] Tey Kok Soon and S. Mekhilef, "A Fast-Converging MPPT Technique for Photovoltaic System Under Fast-Varying Solar Irradiation and Load Resistance," IEEE Trans. Ind. Informat., vol.11, no.1, pp.176-186, 2015.
[25] M. H. Taghvaee, M. A. M. Radzi, S. M. Moosavain, Hashim Hizam and M. Hamiruce Marhaban, "A Current and Future Study on Non-isolated DC–DC Converters for Photovoltaic Applications," Renewable and Sustainable Energy Reviews, vol. 17, pp. 216-227, Jan. 2013.
[26] M. A. Hannan, J. A. Ali, A. Mohamed, U. A. U. Amirulddin, N. M. L. Tan and M. N. Uddin, "Quantum-Behaved Lightning Search Algorithm to Improve Indirect Field-Oriented Fuzzy-PI Control for IM Drive," *IEEE Trans. Ind. Appl.*, vol. 54, no. 4, pp. 3793-3805, July-Aug. 2018.
[27] L. Sheng, G. Xiaojie and Z. Lanyong, "Robust Adaptive Backstepping Sliding Mode Control for Six-Phase Permanent Magnet Synchronous Motor Using Recurrent Wavelet Fuzzy Neural Network," *IEEE Access*, vol. 5, pp. 14502-14515, 2017.